Mechanics of Jointed and Faulted Rock, Rossmanith (ed.) © 1998 Balkema, Rotterdam, ISBN 90 5410 955 6

Seismic wave propagation in fractured rock

Larry Myer
Earth Sciences Division, Ernest Orlando Lawrence Berkeley National Laboratory, Calif., USA

ABSTRACT: The seismic displacement discontinuity model supposes that displacements are locally discontinuous in the plane of a fracture. Normal and shear displacements may be coupled and viscous loss may occur in addition. The consequences of these assumptions on theoretically predicted wavefields are many, including frequency dependent amplitude and velocity changes in transmitted and reflected waves, generations of converted waves and waves trapped as interface waves on the fracture and guided waves between parallel fractures. A number of these characteristics have been observed in laboratory experiments on artificial and natural fractures. Field observations are more limited but have provided evidence of the validity of the model at practical engineering scales.

INTRODUCTION

Rocks contain discontinuities at all scales from grain boundaries and cracks at the microscale to joints and fractures at the macroscale to faults at the mesoscale. It has also been recognized for a long time that the effect of these discontinuities, if averaged over some volume, is a reduction in the stiffness of the rock. From the theory of elasticity for a propagating seismic wave, this reduction in stiffness translates into a reduction in wave velocity. If discontinuities are preferentially oriented in one direction the average stiffness will be reduced more in one direction than another, resulting in an effective anisotropic medium. One of the important characteristics of wave propagation in anisotropic media is that a shear wave propagating at an oblique angle to an axis of symmetry will be split into components traveling at different velocities related to the degree of anisotropy. Thus, shear wave splitting is often taken as diagnostic of fracture orientation and density. These concepts constitute the most common approach in seismic geophysics to modeling wave propagation in fractured rock (e.g. O'Connell and Budiansky 1974, Crampin 1981, Hudson 1981, Thomsen 1996 and others).

A fundamental assumption in this approach is that an appropriate sized volume can be defined over which the effects of the discontinuities can be averaged. This volume is normally defined by wavelength, and it is argued intuitively that if discontinuities are closely spaced compared to wavelength then it is appropriate to use average properties. It is also intuitive to believe that average properties are not meaningful if the wavelength is comparable to, or less than, the average spacing. In this case, the discontinuity must be explicitly modeled. With the advent of piezoelectric and other sources in the kilohertz range, the latter condition is frequently encountered in engineering practice.

This paper will focus on the properties of the seismic wavefield when discontinuities are modeled explicitly. The result is a number of effects which are not predicted by an averaging approach, and can be used to better characterize fractured rock.

THE DISPLACEMENT DISCONTINUITY MODEL

The reduction in stiffness of rock containing a discontinuity arises from excess deformation localized at the discontinuity. Figure 1a is a schematic illustration of the uniaxial loading of a sample containing a discontinuity. Below is a sketch of the average displacement, measured relative to the bottom rigid support. Displacement increases linearly until, at the position of the discontinuity, a local, step increase in displacement occurs. This step increase in displacement, referred to as a displacement discontinuity, is in excess to that which would occur if the sample were intact, as shown schematically in Figure 1b. Though the displacement field is discontinuous, stresses, on average, are continuous. As is well known,

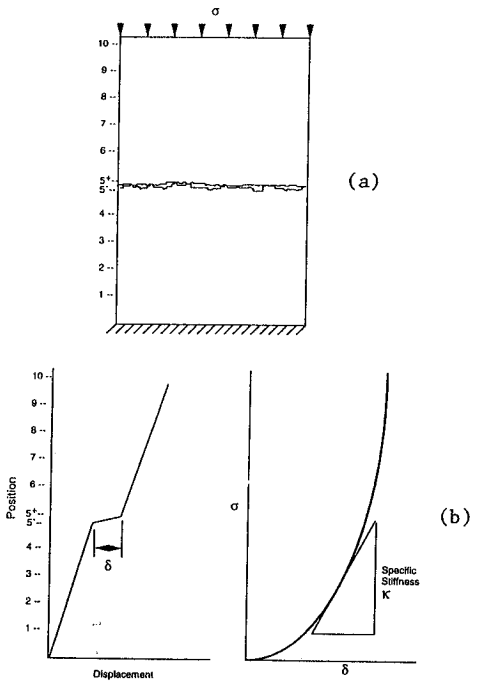

Figure 1. Definition of displacement discontinuity in rock. a) Loading of a sample with a single fracture; b) Left, displacement as function of position, bottom as reference; Right, displacement discontinuity as a function of far field stress.

(Goodman 1976, Bandis et al. 1983, Pyrak-Nolte, et al. 1987) the magnitude of the displacement discontinuity is a nonlinear function of stress. At low stresses, there are few areas of contact between the surfaces of a discontinuity. As stress increases, so do areas of contact so that the displacement discontinuity decreases. The tangent slope to the stress displacement discontinuity curve is referred to as the specific stiffness of the discontinuity.

Generalizing these ideas for dynamic loading under shear as well as normal stress results in the seismic displacement discontinuity boundary conditions (Figure 2):

$$\begin{aligned} u_z^I - u_z^{II} &= \tau_{zz} / \kappa_z, \tau_{zz}^I = \tau_{zz}^{II} \\ u_x^I - u_x^{II} &= \tau_{zx} / \kappa_x, \tau_{zx}^I = \tau_{zx}^{II} \\ u_y^I - u_y^{II} &= \tau_{zy} / \kappa_y, \tau_{zy}^I = \tau_{zy}^{II} \end{aligned} \qquad (1)$$

where
u = particle displacement ($u^I - u^{II} = \delta$)
τ = stress
κ = specific stiffness

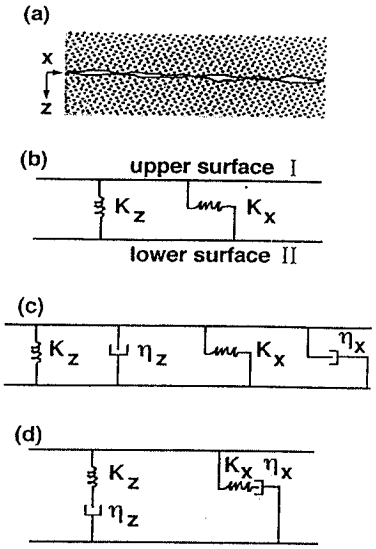

Figure 2. a) Discontinuity; b) Elastic boundary conditions; c) Kelvin rheologic model; d) Maxwell rheologic model.

I,II = superscripts referring to media above and below discontinuity.

These boundary conditions apply over all scales from micro to meso with the restriction that the wavelength is long compared to the spacing between the areas of contact in a discontinuity as well as the size of these areas.

Another assumption in Eq. (1) is that the force displacement relationship in the normal and shear directions are independent. A situation in which this might not be the case is one where the two opposing surfaces of a discontinuity are very rough and loaded in shear. This would result in nonhomogeneous loading on the surfaces and coupling between the normal and shear force displacement relationship. In this case, the boundary conditions for a P- or S_v- wave become

$$\begin{aligned} (u_z^I - u_z^{II})\kappa_{zz} + (u_x^I - u_x^{II})\kappa_{zx} &= \tau_{zz}, \tau_{zx}^I = \tau_{zx}^{II} \\ (u_z^I - u_z^{II})\kappa_{zx} + (u_x^I - u_x^{II})\kappa_{xx} &= \tau_{zx}, \tau_{zz}^I = \tau_{zz}^{II} \end{aligned} \qquad (2)$$

Solutions of the elastodynamic equations for plane waves incident upon a discontinuity modeled by Eq. (1) have been presented by a number of authors (Schoenberg 1980, Pyrak-Nolte et al. 1990, Gu et al. 1996a, and others). The solution including cross coupling terms (Eq. 2) is discussed in Nakagawa 1998 and Myer et al. 1998. Figure 3 presents results for the case of normal incidence in which $|T|$ is the magnitude of the transmission

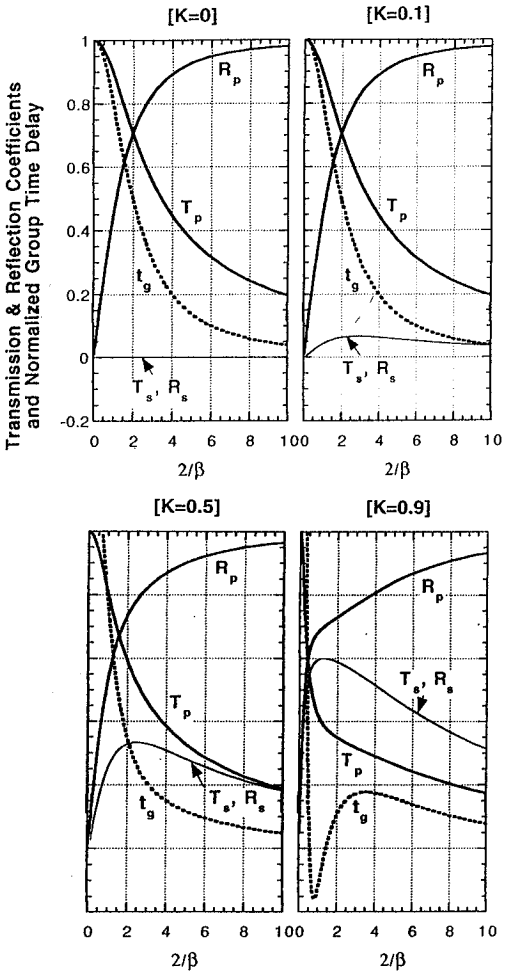

Figure 3. Magnitude of transmission and reflection coefficients and group time delay for P-wave normally incident upon an elastic interface with cross coupled stiffness.

coefficient, $|R|$ is the magnitude of the reflection coefficient and t_g is a normalized group time delay for the transmitted wave. The parameter

$$\beta \equiv \frac{z\kappa_{zz}/\omega}{z_p}$$

where

ω = angular frequency
$z_p = \rho c_p$ for P-waves
$c_p = \sqrt{\lambda + 2\mu/p}$
ρ = density
λ,μ = Lame's constants for media on either side of discontinuity

Plots are shown for a range of the values of the ratio $K = \kappa_{zy}/\kappa_{zz}$. For $K = 0$ the cross coupling stiffness terms are zero, corresponding to the solution for conditions given by Eq. (1).

Results in Figure 3 show that the seismic displacement discontinuity model predicts that a single joint or fracture should cause a frequency dependent change in the amplitude and velocity of a propagating seismic wave. High frequency components of a wave are preferentially reflected. Because the discontinuity is elastic, as described by Eqs. (1) or (2), there is no energy dissipation; energy is either transmitted or reflected. The curve for t_g implies that high frequency components are slowed less than low frequency components.

The effect of nonzero cross coupling terms is to generate converted waves. For the case of a normally incident P-wave as shown in Figure 3, transmitted and reflected S-waves are formed with amplitudes which are frequency and stiffness dependent. The negative values of t_g in one panel imply that, under some conditions, the P-wave velocity could be increased.

Limiting conditions for the displacement discontinuity model occur for specific stiffness approaching zero or infinity. For $\kappa \to 0$, the solution reverts to that for a plane wave incident upon a free boundary, and for $\kappa \to \infty$ the solution is equivalent to those of classical seismology in which both displacements and stresses are continuous at the boundaries between layers.

The elastic boundary conditions do not account for energy dissipation which could occur due to partial saturation or clay in the discontinuity. Two very simple rheological models which also have practical significance are the Kelvin and Maxwell models. For Kelvin rheology Eqs. (1) become:

$$(u_z^I - u_z^{II})(\kappa_z - i\omega\eta_z) = \tau_{zz},\ \tau_{zz}^I = \tau_{zz}^{II}$$
$$(u_x^I - u_x^{II})(\kappa_x - i\omega\eta_x) = \tau_{zx},\ \tau_{zx}^I = \tau_{zx}^{II}$$
$$(u_y^I - u_y^{II})(\kappa_y - i\omega\eta_y) = \tau_{zy},\ \tau_{zy}^I = \tau_{zy}^{II} \qquad (3)$$

and for Maxwell rheology:

$$(u_z^I - u_z^{II}) = \tau_{zz}\left(\frac{1}{\kappa_z} + \frac{i}{\omega\eta_z}\right),\ \tau_{zz}^I = \tau_{zz}^{II}$$
$$(u_x^I - u_x^{II}) = \tau_{zx}\left(\frac{1}{\kappa_x} + \frac{i}{\omega\eta_x}\right),\ \tau_{zx}^I = \tau_{zx}^{II}$$
$$(u_y^I - u_y^{II}) = \tau_{zy}\left(\frac{1}{\kappa_y} + \frac{i}{\omega\eta_y}\right),\ \tau_{zy}^I = \tau_{zy}^{II} \qquad (4)$$

where
K = specific viscosity (units of viscosity per length).

The magnitude of the transmission and reflection coefficient for a normally incident wave are plotted in Figure 4. The solution becomes equivalent to that of the elastic interface when the specific viscosity becomes large (e.g. $z/2\eta = 0.01$). When the specific viscosity is small (e.g. $z/2\eta = 5$), the solution is dominated by the viscous element. Thus, both $|T|$ and $|R|$ become frequency independent. Since energy is lost by viscous dissipation at the discontinuity, $|R|^2 + |T|^2 \neq 1$.

For oblique angles of incidence of P- or S_v plane wave, the displacement discontinuity model predicts that converted waves will be generated even though the material properties on either side of the discontinuity are the same. Snell's law defines the relationship between the angles of incidence, reflection, and refraction. For S_v incident waves, a critical angle exists above which transmitted and reflected waves are no longer real valued. Transmissions and reflection coefficients for oblique angles of incidence have been developed by several authors (Schoenberg 1980, Pyrak-Nolte et al. 1990, Gu et al. 1996a and others).

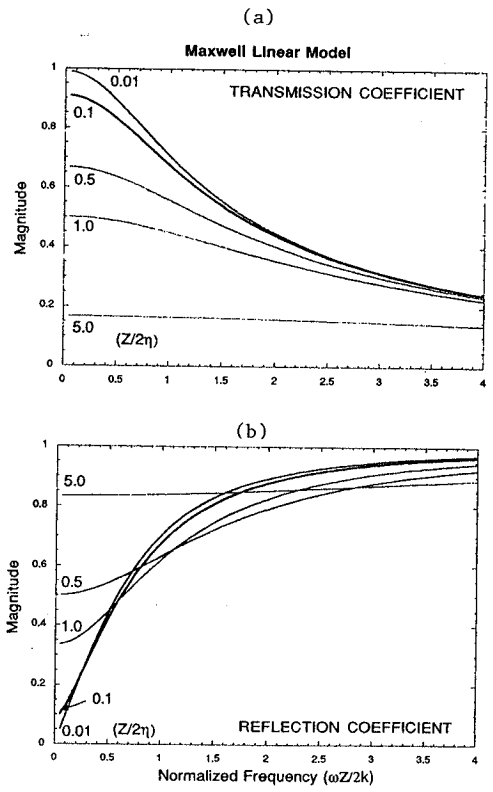

Figure 4. a) Magnitude of the transmission coefficient for normal incidence assuming Maxwell rheologic model for boundary conditions; b) Magnitude of the reflection coefficient.

It is well known that energy will propagate along a free surface as a Rayleigh wave or, under some conditions, along an interface between materials of contrasting properties (Stoneley 1924). It is now recognized that a discontinuity such as a fracture will support an interface wave even though the materials on either side of the discontinuity have the same properties. Solutions for an inhomogeneous plane wave propagating along a discontinuity described by the elastic displacement discontinuity model have been obtained by Pyrak-Nolte and Cook 1987, Gu et al. 1996b, Nihei et al. 1995 and others. Two interface waves are predicted with phase velocities which lie between the Rayleigh wave and shear body wave velocities and are dependent upon the specific stiffness of the discontinuity. The particle motion of these waves is elliptic and exponentially decays in amplitude with distance from the discontinuity. These waves are therefore known as generalized Rayleigh waves.Boundary element simulations for point sources located on or near a discontinuity (Gu et al. 1996b) showed that an interface wave traveling at a velocity close to the P-body wave should exist in addition to the generalized Rayleigh waves.

Figure 5 presents waveforms for a cylindrical source located on an elastic discontinuity of varying specific stiffness. At very high stiffness, only a P-wave is present, representing the response of the medium without a discontinuity. As specific stiffness decreases a generalized Rayleigh wave and a P-interface wave develop.

Finally, Nihei et al. 1994 and Nihei et al. 1998 have shown that energy can be trapped as guided waves between two fractures even though there are no material property contrasts. A family of dispersive trapped wave modes is predicted for each value of specific stiffness. The modes have x-component particle notion which is either symmetric or antisymmetric with respect to the center of the waveguide. Figure 6 shows particle motions for the lowest order antisymmetric mode for two values of specific stiffness of the discontinuities. For low values of specific stiffness, most energy is trapped between the discontinuities. As specific stiffness increases, more energy couples across the discontinuities indicating a transition to the bulk body wave.

Neither interface waves nor guided waves are predicted if the classical approach of replacing a fractured medium by effective anisotropic properties is followed. If such waves exist in practice, they could be diagnostic of fracturing at scales of interest in many engineering projects. Observations of these waves at laboratory and field scale is discussed below.

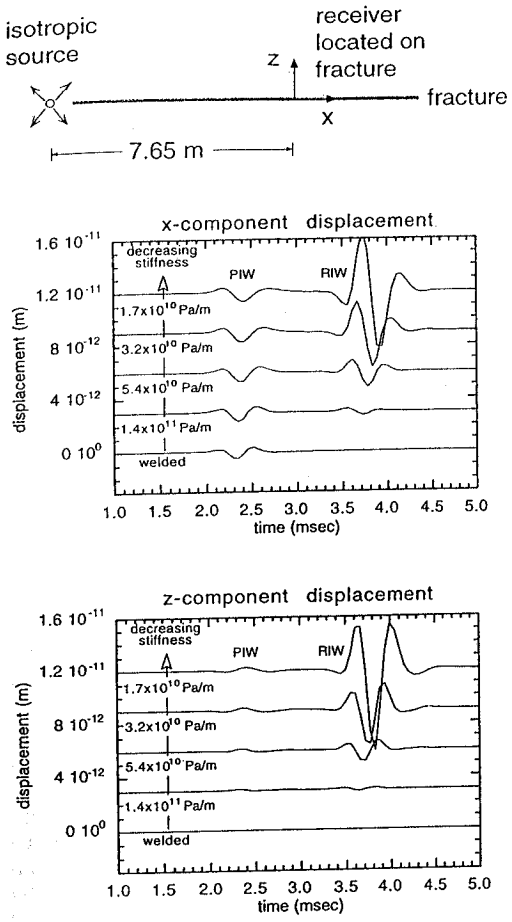

Figure 5. x and z components of particle displacements for different values of fracture specific stiffness from boundary element simulation.

LABORATORY MEASUREMENTS

The displacement discontinuity model for normal incidence waves has been validated in laboratory measurements on idealized fractures formed by lead foil strips sandwiched between two steel cylinders placed end to end (Myer et al. 1985). A reference measurement was made in which a solid disk of the foil was placed between the cylinders. Strip thickness (0.03 mm), width (1.0 mm), and spacing (variable from 1 mm to 7 mm) were small compared to wavelength (23 mm for P-wave at center frequency). The strips were placed in parallel, effectively forming a coplanar array of cracks (Figure 7). For such a geometry analytic expressions can be used to calculate the stiffness and magnitude of the displacement discontinuity, δ, (Tada et al. 1973, Myer et al. 1995 and others).

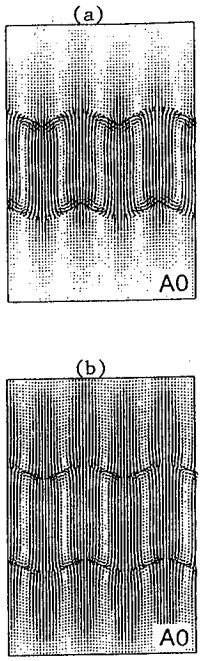

Figure 6. Predicted mode shapes for the lowest order antisymmetric fracture channel wave for a frequency of 1 kHz, P-wave velocity of 3118 m/s, S-wave velocity of 1800 m/s; a) specific stiffness of $1 \times 10^9 P_a/m$; b) specific stiffness of $1 \times 10^{10} P_a/m$.

The "predicted" curves in Figure 7 were therefore generated without "adjustable" variables. The magnitude of the transmission coefficient, $|T|$, as a function of frequency, is uniquely determined from the calculated stiffness. The product of $|T|$ and the measured spectral amplitudes for the reference test yields the predicted spectral amplitudes. It should be noted that previous reference to these lead foil strip tests (Myer et al. 1985 and Myer et al. 1995) presented results for s-wave transmission which were erroneously labeled as P-wave results. Subsequent tests were performed in which lead strips were used to form two parallel idealized fractures. Results showed that, for widely spaced fractures, the magnitude of the transmission coefficient for a wave propagating across a set of parallel fractures is $|T|^N$ where $|T|$ is the value for a single fracture and N is the number of fractures (Myer et al. 1995).

The displacement discontinuity model has been used to successfully simulate laboratory P- and S-wave transmission measurements on specimens containing single natural fractures (Pyrak-Nolte et al. 1990). The frequency dependent reduction in amplitude of waves transmitted across the fractures varied with the amount of normal stress applied to

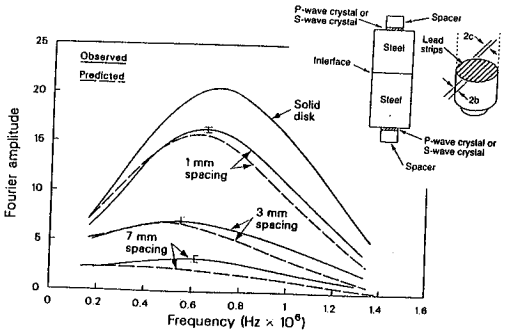

Figure 7. Amplitude spectra obtained from experiment compared with those predicted using "solid disk" spectrum as reference.

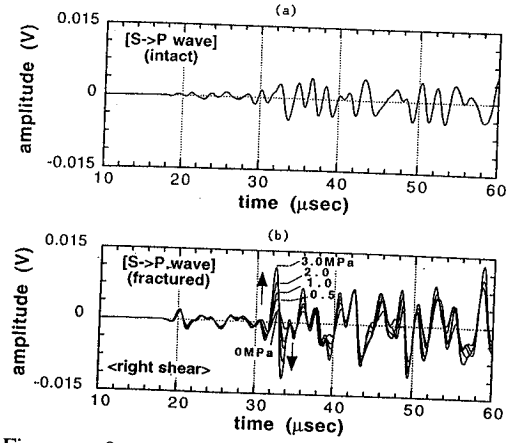

Figure 8. Waveforms from experiment demonstrating stiffness crosscoupling; a) P-wave receiver receiver response for intact sample; b) P-wave receiver response for fractured sample with shear stress applied to generate first motion indicated by arrows.

the fractures, reflecting the effect of changes in specific stiffness as illustrated in Figure 1. Good agreement between observed and modeled results was achieved by using values of fracture stiffness of the same order of magnitude, though somewhat higher than those measured under pseudostatic loading conditions. Elastic boundary conditions in the displacement discontinuity model well simulated P- and S-wave propagation across dry natural fractures and P-wave propagation across water saturated fractures. S-wave propagation across water saturated fractures was better simulated by assuming rheologic boundary conditions (Pyrak-Nolte et al. 1990).

Evidence for the existence of converted waves formed due to cross-coupling terms in the stiffness matrix has been provided by laboratory tests by Nakagawa 1998. A piezoelastic S-wave source was placed at one end of a cylindrical granite sample and a piezoelastic P-wave receiver at the opposite end. The received waveform for the intact specimen as shown in Figure 8a constituted a reference signal. The sample was then fractured under Brazilian loading creating a fracture perpendicular to the axis of the sample. A shear load was imposed on the fracture and the transmission experiment repeated. Results (Figure 8b) show the arrival of a converted P-wave which grows in amplitude as shear stress on the fracture increases. The increasing shear stress created an asymmetric loading on asperities of contact in the fracture plane and, consequently, cross coupled stiffness terms.

Fluids of differing chemistries and clay coatings of differing mineralogy are ubiquitous in fractured rock systems. The presence of these additional components not only changes the stiffness of a fracture but also can result in dissipation of energy. Suárez-Rivera 1992 and Suárez-Rivera et al. 1992 explored the effects of clay coatings on propagation of S-waves across fractures and found that even thin clay coatings can cause significant attenuation if the clays absorb pore fluids, or, in civil engineering terms, are prone to swelling behavior. He further found that the displacement discontinuity model incorporating rheologic boundary conditions well simulated the result of laboratory experiments. Figure 9 shows the results of the transmission and reflection of an S-wave by a thin Na-montmorillonite layer containing 27% water by weight. The clay layer was about 5μm thick and was sandwiched between quartz disks. The reference spectrum refers to the case when no clay was present for the transmitted wave and a free surface was present for the reflected wave. Measurements were made at different levels of load applied normal to the quartz disks confining the layer. Experimental results were well simulated assuming a Maxwell rheologic model in which single values of specific stiffness and specific viscosity were used to fit the transmitted, reflected and viscous loss spectral data at each normal load.

Laboratory confirmation of the existence and properties of fracture interface waves has been carried out by several investigators. Pyrak-Nolte et al. (1992) placed two aluminum blocks together, forming an interface or idealized fracture between them. Both slow and fast interface waves were observed. It was also shown, in accordance with theory, that no interface wave is present for source shear motion in the plane of the fracture (S_h source). In similar tests on rock fracture, Rayleigh-type interface waves have been observed by Ekern et al.

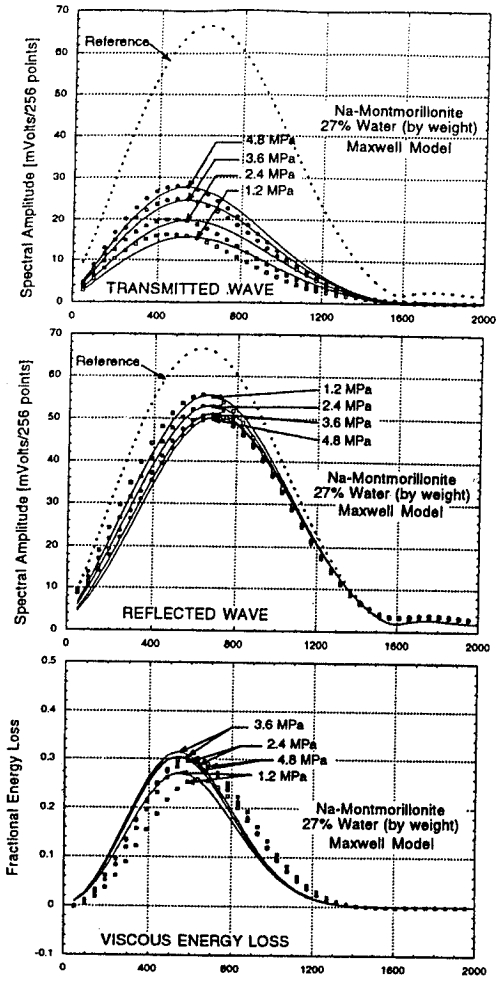

Figure 9. Comparison of observed and predicted amplitude spectra and energy loss for shear waves propagated across a thin layer of clay for different values of normal stress on the clay layer. Predicted values based on Maxwell model and the indicated reference spectra.

1995 and Roy and Pyrak-Nolte 1995. A compressional-mode interface wave was observed by Roy and Pyrak-Nolte 1997. Using a sheet of Plexiglas containing a single idealized fracture, Fan et al. (1996) confirmed particle motion patterns and decay in amplitude away from a discontinuity as predicted by theory.

Nihei et al. (1998) have recently demonstrated at laboratory scale the existence of trapped waves in a channel formed by two fractures. Two parallel fractures were generated in a 30.5 cm square by 1.05 cm thick slab of marble. A piezoelectric shear source was placed on the edge of the slab and located midway between the fractures. Particle motions were mapped on the surface of the slab and are shown in Figure 10 a,b for two different levels of normal stress across the fractures. The particle motions are consistent with the lowest order antisymmetric mode (see Figure 6). At the higher stress, Figure 10b, larger amplitudes were observed outside the channel formed by the fractures. At the higher stress, the specific stiffness of the fractures was higher, allowing coupling of energy outside the channel, in accordance with theory.

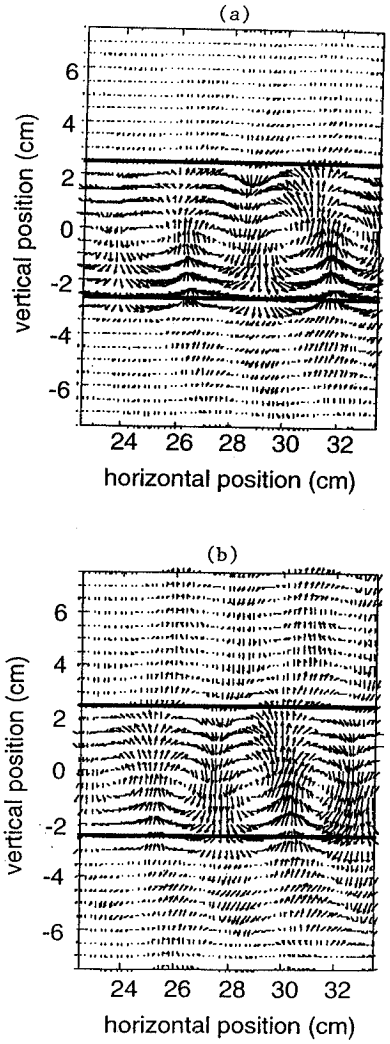

Figure 10. Measured particle motions in a fractured marble plate; a) Low normal stress across fractures; b) Higher normal stress

FIELD OBSERVATIONS

A small scale cross-well test performed in basalt provided some of the first evidence for applicability of the displacement discontinuity model at field scale (King et al. 1986, Myer et al. 1995). Measurements were made between horizontal drill holes, labeled C1, C2, C3, C4, as shown in Figure 11a, spaced 3m apart in the wall of a drift above the water table. The primary fracture set as shown in the figure was formed by the basalt columns which ranged in thickness from about 0.2m to 0.4m. Crosswell measurements were made with a 1.0m source and receiver spacing. The effect of propagating across the column-forming fractures is shown in Figure 11b, which presents first arriving P-wave pulses for different borehole pairs. Pulses which crossed column-forming fractures were slowed and attenuated compared to those propagating along a column, qualitatively in accordance with predictions of the displacement discontinuity model.

Results of quantitative modeling of four of the C2-C4 crosswell raypaths are shown in Figure 11c. The modeling procedures consisted of first selecting a reference pulse from the data set for the C1-C2 measurements. After transforming into the frequency domain and correcting for path length and intrinsic attenuation in the rock mass, this spectrum was multiplied by the transmission coefficient assuming elastic boundary conditions in the displacement discontinuity model. The result was inverse transformed to the time domain for comparison with the observed pulses. The number of fractures at each raypath location was held constant (at 3) while fracture stiffness was changed to obtain the best fit with observations. The stiffness varied between 1.0×10^{11} and 5.0×10^{11} mPa/m units for the results shown. It is seen that the simple elastic model captures quite well the amplitude reduction, dispersion and time delay experienced by the pulses which crossed the fractures between C2 and C4.

More recent crosswell measurements in a shallow fractured limestone formation provide evidence of the existence of fracture interface waves at field scale. A comprehensive set of high resolution (1 to 10kHz) crosswell measurements have been obtained between five vertical wells (Majer et al. 1997). Majer et al. also found that a single, strata-bound vertical fracture with strike as shown in Figure 12a intersected well GW-5. For source positions in GW-5 an arrival corresponding to an interface wave would be expected in GW-2, which is also located on, or immediately adjacent to, the fracture. The arrival in GW-2 interpreted as the interface wave is marked in Figure 12b. The delay time for this arrival is also consistent with results of a theoretical

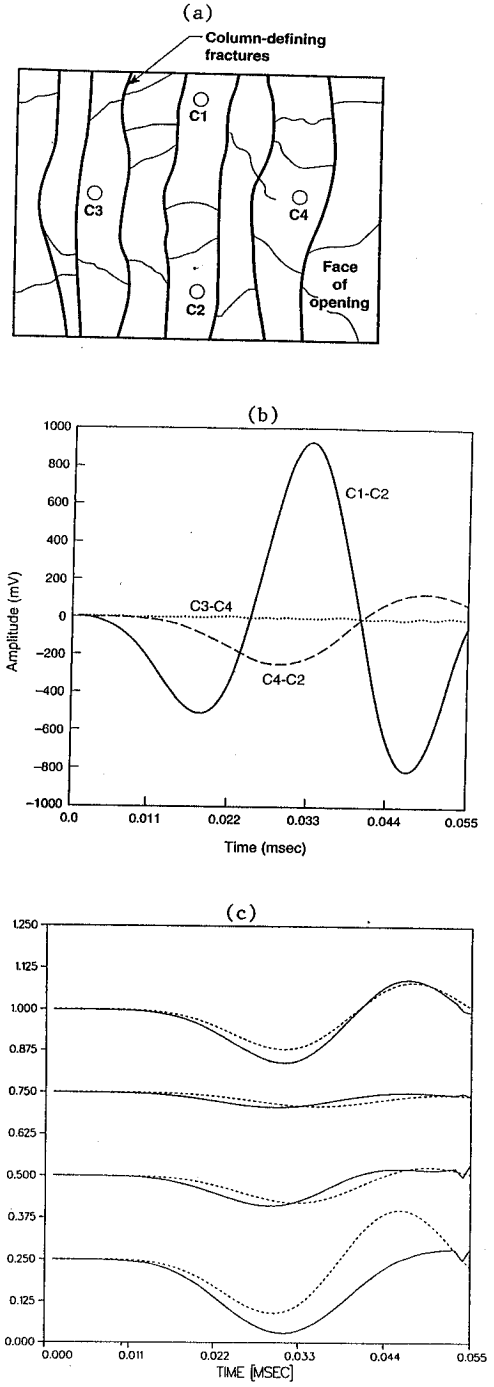

Figure 11. a) Borehole configuration in fractured basalt; b) comparison of pulses propagating between different borehole combinations; c) Modeling (dashed lines) of four pulses from C4-C2 data set.

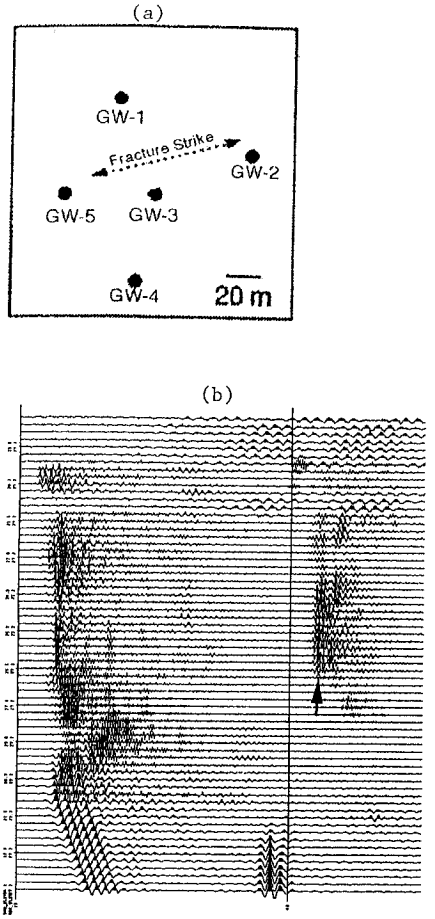

Figure 12. a) Plan view of well locations; b) GW-5 to GW-2 crosswell results; arrow indicating arrival of interface wave; c) GW-3 to GW-4 crosswell results.

model (see Figure 5) constructed with source characteristics and rock properties relevant to the in-situ test.

CONCLUSIONS

When the wavelengths are comparable to or less than the average spacing of discontinuities it is no longer appropriate to average their effects on wave propagation. The displacement discontinuity model has been shown to capture many aspects of the physics associated with the interaction of seismic waves with individual discontinuities. Theoretical studies have defined the transmission and reflection characteristics of plane waves propagating across elastic and rheologic discontinuities. Propagation parallel to discontinuities results in energy being trapped as interface and guided waves. Such waves are not predicted by effective media approaches.

Laboratory studies have validated many aspects of the displacement discontinuity model through measurements of transmission and reflection of plane waves incident on elastic and rheologic discontinuities. Laboratory measurements also established the existence and properties of interface and guided waves which had not previously been redognized.

Field observations and applications of the displacement discontinuity model are few. The model provides potential for improved characterization of fractured rock, but implementation will require further development of interpretational tools.

ACKNOWLEDGMENTS

I would like to acknowledge Professor Neville Cook, past and present graduate students and my colleagues, particularly Dr. Kurt Nihei, without whom the concepts in this paper would not have progressed. I also acknowledge Dr. John Queen and others at CONOCO for their collaborative contribution to in-situ testing of these concepts. I thank Dr. Nihei for numerical results shown in Figure 5 and Dr. John Peterson for results shown in Figure 11. The work was carried out under U.S. Department of Energy Contract No. DEA03-76SF00098. Support was provided by the Director, DOE Office of Energy Research, Office of Basic Energy Science, the Director, DOE Office of Fossil Energy, Office of Oil, Gas and Shale Technologies, and the Gas Research Institute.

REFERENCES

Bandis, S.C., A.L. Lumsden & N.R. Barton 1983. Fundamentals of rock joint deformation. *Int. J. of Rock Mechanics and Mining Sciences & Geomechanical Abstracts* 20(6):249-268.

Crampin, S. 1981. A review of wave motion in anisotropic and cracked elastic media. *Wave Motion* 3:343-391.

Ekern, A., R. Suárez-Rivera & A. Hansen 1995. Investigation of interface wave propagation along planar fractures in sedimentary rocks. In J. Daemen & R. Schultz (eds), *Rock Mechanics, Proceedings of the 35th U.S. Symposium* 161-167, Balkema.

Fan, J., B. Gu, K.T. Nihei, N.G.W. Cook & L.R. Myer 1996. Experimental and numerical investigation of fracture interface waves. In M. Aubertin, R. Hassani, & H. Mitri (eds), *Rock Mechanics, Tools and Techniques, Proceedings*

of 2nd North American Rock Mechanics Symposium 1:845-851.

Goodman, R.E. 1976. *Methods of Geological Engineering Discontinuous Rock.* St. Paul: West Publishing Co.

Gu, B., R. Suárez-Rivera, K. Nihei & L.R. Myer 1996a. Incidence of plane waves upon a fracture. *J. Geophys. Res.* 101(B11):25337-25346.

Gu, B., K. Nihei, L. Myer & L. Pyrak-Nolte 1996b. Fracture interface waves. *J. Geophys. Res.* 101(B1):827-835.

Hudson, J.A. 1981. Wave speeds and attenuation of elastic waves in material containing cracks. *Geophys. J.R. Astron Soc.* 64(1):133-150.

King, J.S., L.R. Myer & J.J. Rezowalli 1986. Experimental studies of elastic-wave propagation in a columnar-pointed rock mass. *Geophysical Prospecting* 34(8):1185-1199.

Majer, E.L., J.E. Peterson, T. Daley, B. Kaelin, L. Myer, J. Queen, P. D'Onfro & W. Rizer 1997. Fracture detection using crosswell and single well surveys. *Geophysics* 62(2):495-504.

Myer, L.R., D. Hopkins & N.G.W. Cook 1985. Effects of contact area of an interface on acoustic wave transmission. In *Research and Engineering Application in Rock Mechanics, Proceedings of the 26th U.S. Symposium on Rock Mechanics* 549-556. Rotterdam: Balkema.

Myer, L.R., D. Hopkins, J. Peterson & N. Cook 1995. Seismic wave propagation across multiple fractures. In Myer, Cook, Goodman and Tsang (eds), *Fractured and Jointed Rock Masses*:105-110. Rotterdam: Balkema.

Myer, L.R., K.T. Nihei & S. Nakagawa 1998. Dynamic properties of interfaces. H.P. Rossmanith (ed), *Damage and Failure of Interfaces*. Balkema (in press).

Nakagawa, S. 1998. Acoustic resonance characteristics of rock and concrete including fracture, *Ph.D. Thesis*, University of California, Berkeley.

Nihei, K.T., L.R. Myer, N.G.W. Cook & W. Yi 1994. Effects of non-welded interfaces on guided SH-waves. *Geophysical Research Letters* 21(9):745-748.

Nihei, K.T., B. Gu, L.R. Myer, L.J. Pyrak-Nolte & N.G.W. Cook 1995. Elastic interface wave propagation along a fracture. *Proc. 8th Int. Cong. Rock Mech., Tokyo, 25-29 Sept 1995*:Rotterdam: Balkema.

Nihei, K.T., W. Yi, L.R. Myer & N.G.W. Cook 1998. Fracture channel waves. *J. of Geophysical Research*, submitted.

O'Connell, R.J. & B. Budiansky 1974. Seismic velocities in dry and saturated cracked solids. *J. Geophys. Res.* 79:5412-5426.

Pyrak-Nolte, L.J. & N.G.W. Cook 1987. Elastic interface waves along a fracture. *Geophys. Res. Lett.* 14:1107-1110.

Pyrak-Nolte, L.J., L.R. Myer, N.G.W. Cook & R.A. Witherspoon 1987. Hydraulic and mechanical properties of natural fractures in low permeability rock. *Proceedings of 6th International Congress of Rock Mechanics*: I:225-232, Rotterdam:Balkema.

Pyrak-Nolte, L.J., L.R. Myer & N.G.W. Cook 1990. Transmission of seismic waves across single natural fractures. *J. Geophys. Res.* 95:8617-8638.

Pyrak-Nolte, L.J., J. Xu & G. Haley 1992. Elastic interface waves propagating in a fracture. *Physical Review Letters* 69(24):3650-3653.

Roy, S. & L.J. Pyrak-Nolte 1995. Interface waves propagating along tensile fractures in dolomite. *Geophysical Research Letters* 22(20):2773-2776.

Roy, S. & L.J. Pyrak-Nolte 1997. Observation of a distinct compressional-mode interface wave on a single fracture. *Geophysical Research Letters* 24(2):173-176.

Schoenberg, M. 1980. Elastic wave behavior across linear slip interfaces. *J. Acoust. Soc. Am.* 68(5):1516-1521.

Stoneley, R. 1924. Elastic waves at the surface of separation of two solids. *Proceedings of the Royal Society, London.* 106:416-428.

Suárez-Rivera, R. 1992. The influence of thin clay layers containing liquids on the Propagation of shear waves. *Ph.D. Thesis*, University of California, Berkeley.

Tada, H.P., P.C. Paris & G.K. Irwin 1973. *The stress analysis of cracks handbook.*Helbertown, PA: Del Research Corp.

Thomsen, L. 1986. Weak elastic anisotropy. *Geophysics* 51(10):1954-1966.